# Angular Velocity-based Structural Damage Detection

Yizheng Liao[a] and Anne S. Kiremidjian[b] and Ram Rajagopal[a] and Chin-Hsiung Loh[c]

[a]Stanford Sustainable Systems Lab, Department of Civil and Environmental Engineering, Stanford University, 473 Via Ortega, Stanford, CA, United States;
[b]Department of Civil and Environmental Engineering, Stanford University, 473 Via Ortega, Stanford, CA, United States;
[c]Department of Civil Engineering, National Taiwan University, No.1, Section 4, Roosevelt Road, Taipei 10617, Taiwan;

## ABSTRACT

Damage detection is an important application of structural health monitoring. With the recent development of sensing technology, additional information about structures, angular velocity, has become available. In this paper, the angular velocity signals obtained from gyroscopes are modeled as an autoregressive (AR) model. The damage sensitive features (DSFs) are defined as a function of the AR coefficients. It is found that the mean values of the DSF for the damaged and undamaged signals are different. Also, we show that the angular velocity-based AR model has a linear relationship with the acceleration-based AR model. To test the proposed damage detection method, the algorithm has been tested with the experimental data from a recent shake table test where the damage is introduced systemically. The results indicate that the change of DSF means is statistically significant, and the angular velocity-based DSFs are sensitive to damage.

**Keywords:** Damage Detection, Structural Health Monitoring, Angular Velocity, Wireless Sensor Network

## 1. INTRODUCTION

Structural health monitoring (SHM) has become great significant in the field of civil engineering during the last two decades. Since many civil infrastructures, such as bridges and buildings, are exposed to complex loadings and environment, it is necessary to continuously monitor the performance level and safety of structures during daily operation and extreme events like earthquakes and hurricanes.

Among different types of SHM methodology, the vibration-based damage detection algorithms using acceleration measurements have received considerable attention. When the physical properties, such as mass and stiffness, are changed, the structural modal properties (e.g. natural frequency, mode shapes) will become different as well. Therefore, damage can be detected by comparing the features extracted from the structural responses before and after damage. Comprehensive summaries and discussions on the vibration-based damage detection are given in Ref.1–3.

Recently, with the development of sensing technology, many new low-cost microelectromechanical sensors (MEMS) become available. These sensors provide many new structural quantities, which are not available or expensive to measure before. Recent research works have demonstrated that these newly available information could improve the reliability and accuracy of structural damage detection.[4,5] For example, many off-the-shelf sensors have both accelerometers and gyroscopes on board now. They are synchronized and provide measurements simultaneously. Therefore, we can use the angular velocity to complement the acceleration-based damage detection.

In this paper, we propose a damage detection algorithm based on the newly available angular velocity measurements. We firstly formulate the angular velocity signal as an autoregressive (AR) model and use the model

Further author information: (Send correspondence to Yizheng Liao)
Yizheng Liao: E-mail: yzliao@stanford.edu
Anne S. Kiremidjian: E-mail: ask@stanford.edu
Ram Rajagopal: E-mail: ramr@stanford.edu
Chin-Hsiung Loh: Email: lohc0220@ccms.ntu.edu.tw

coefficients as the damage sensitive feature (DSF). Then we discuss the connection between the acceleration-based AR model and angular velocity-based AR model. Our results show that the coefficients of both AR models have a linear relationship. Therefore, we can extend the statistical properties of the acceleration-based AR model to the new DSF. Thirdly, we use the data collected from a recent shake table test to validate the sensitivity of the angular velocity-based DSFs to damage. The results indicate that the difference in the means of the DSFs before and after the damage is significant.

The rest paper is organized as follows: Section 2 presents the AR model of the angular velocity signal and shows the connection with the acceleration-based AR model; Section 3 validates the angular velocity-based DSFs on an experimental data set; Section 4 draws the conclusion.

## 2. ANGULAR VELOCITY-BASED DAMAGE DETECTION ALGORITHM

The proposed angular velocity-based algorithm consists of three steps: (i) data acquisition, (ii) damage sensitive feature (DSF) extraction, and (iii) damage identification and classification. This process is summarized in Fig. 1. In this first step, structural responses, either acceleration or angular velocity, are obtained sequentially. In this paper, SnowFort, an open source wireless sensor network for infrastructural monitoring,[6] is used as the data acquisition system. Details are given in Section. 3. In the second step, we apply the auto-regressive (AR) model to extract the DSF. Then the statistical method is applied to declare damage. In this paper, we perform the hypothesis test to identify damage.


Figure 1. Flow chart of the proposed algorithm

### 2.1 Feature Extraction

The DSF extraction includes two steps: (i) normalization and standardization and (ii) AR model fitting. The discrete time angular velocity responses from sensor $j$, $\omega_j[n]$, is divided into chunks with a size $N$. Let $\omega_j^i[n]$ denote the $i$th chunk of the signal $\omega_j[n]$. The normalized and standardized signal $\tilde{\omega}_j^i[n]$ is obtained as follows:

$$\tilde{\omega}_j^i[n] = \frac{\omega_j^i[n] - \mu_j^i}{\sigma_j^i},$$

where $\mu_j^i$ and $\sigma_j^i$ denote the mean and standard deviation of the $i$th chunk. For notation convenience, we will use $\omega_j^i[n]$ as $\tilde{\omega}_j^i[n]$ in the following text.

The AR model has been used to model the time-series structural responses by many previous works.[7–9] The singe-variate AR model of order $p$ is given as

$$\omega_j^i[n] = \sum_{k=1}^{p} \beta_k \omega_j^i[n-k] + \epsilon[n], \tag{1}$$

where $\beta_k$ is the $k$th AR coefficient and $\epsilon[n]$ is the residual and follows a Gaussian distribution with mean 0 and variance $\sigma^2$. The AR coefficients $\beta_k$ will serve as the DSF in our damage detection algorithm. In the following section, we will show that the coefficients of angular velocity-based AR model are sensitive to the damage.

### 2.2 AR model of angular velocity

In previous work, the coefficients of the acceleration-based AR model have been widely used as the DSF because they are closely related to structural parameters[7] and sensitive to damage.[8,10] In this section, we will show that the coefficients of the angular velocity-based AR model are also sensitive to damage.

Let $a[n]$ denote the discrete time acceleration signal at time $n$. We assume that the acceleration signal has been standardized and normalized. The acceleration-based AR model of order $p$ is given as

$$a[n] = \sum_{k=1}^{p} \alpha_k a[n-k] + \delta[n], \tag{2}$$

where $\alpha_k$ is the $k$th AR coefficient and $\delta[n]$ is the residual and follows a Gaussian distribution with mean 0 and variance $\tilde{\sigma}^2$. At time $n$, the velocity $v[n]$ can be expressed as

$$v[n] = v[n-1] + Ta[n], \tag{3}$$

where $T_s = \frac{1}{f_s}$ is the sampling rate and $f_s$ is the sampling frequency. With substitution, (2) becomes to

$$\frac{v[n]-v[n-1]}{T_s} = \sum_{k=1}^{p} \alpha_k \frac{v[n-k]-v[n-k-1]}{T} + \delta[n] \tag{4}$$

$$\begin{aligned} v[n]-v[n-1] &= \sum_{k=1}^{p} \alpha_k (v[n-k]-v[n-k-1]) + T_s\delta[n] \qquad (5)\\ &= \alpha_1 v[n-1] + (\alpha_2-\alpha_1)v[n-2] + \cdots + (\alpha_p - \alpha_{p-1})v[n-p] - \alpha_p v[n-p-1] + T_s\delta[n] \\ v[n] &= (\alpha_1+1)v[n-1] + (\alpha_2-\alpha_1)v[n-2] + \cdots + (\alpha_p - \alpha_{p-1})v[n-p] - \alpha_p v[n-p-1] + T_s\delta[n] \\ &= \sum_{k=1}^{p+1} \tilde{\alpha}_k v[n-k] + \tilde{\delta}[n], \qquad (6) \end{aligned}$$

where $\tilde{\delta}[n]$ is a Gaussian random variable with zero mean and a variance of $T_s^2\tilde{\sigma}^2$.

The angular velocity $\omega[n]$ has a linear relationship with the linear velocity $v[n]$, as follows:

$$\omega[n] = \frac{v[n]}{r},$$

where $r$ is the constant radius. The gyroscope measures the rotation speed around the vertical axis of the acceleration, as shown in Fig. 2. Therefore, the AR model of angular velocity is

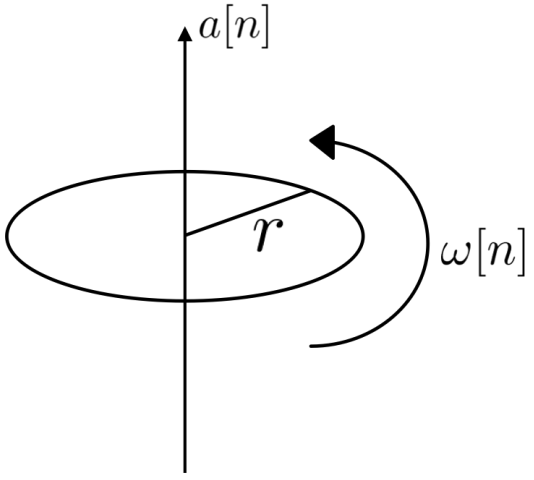


Figure 2. Relationship between the acceleration ($a[n]$) and the angular velocity ($\omega[n]$).

$$
\begin{aligned}
w[n] &= \frac{1}{r}v[n] \\
&= \frac{1}{r}\left(\sum_{k=1}^{p}\tilde{\alpha}_k v[n-k] + \tilde{\delta}[n]\right) \\
&= \sum_{k=1}^{p}\tilde{\alpha}_k \frac{v[n-k]}{r} + \frac{1}{r}\tilde{\delta}[n] \\
&= \sum_{k=1}^{p}\tilde{\alpha}_k \omega[n-k] + \frac{1}{r}\tilde{\delta}[n] \qquad (7) \\
&= \sum_{k=1}^{p}\beta_k \omega[n-k] + \epsilon[n]. \qquad (8)
\end{aligned}
$$

Therefore, the first AR coefficient of the angular velocity-based model is a linear shift of the first coefficient of the acceleration-based AR model, i.e. $\beta_1 = 1 + \alpha_1$. The rest coefficients of the angular velocity-based AR model is the difference of the coefficients of the acceleration-based AR model, i.e. $\beta_i = \alpha_i - \alpha_{i-1}$. The variance of the residual term in the angular velocity-based AR model is a scaled version of the term in the acceleration-based AR model, i.e. $\sigma^2 = T_s^2\tilde{\sigma}^2$.

In the acceleration-based AR model, the damage is identified by investigating the difference of means of DSFs before and after damage.[7] As shown in (6) and (8), the coefficients of angular velocity-based AR model are a linear combination of $\alpha$. Therefore, the means of coefficients in the angular velocity-based AR model will be different before and after damage. In Section. 3, we will show the means before and after damage. Also, since the acceleration-based AR coefficients follow the Gaussian distribution,[11] the angular velocity-based AR coefficients will follow the Gaussian distribution as well due to the linear transformation in (6). Furthermore, since $T_s \ll 1$ in many cases, the variance of noise term in the angular velocity-based AR model is much smaller than that in the acceleration-based model. It means that the new model can achieve the same accuracy with the lower order. In many applications, the AR fitting algorithm is embedded on the low-power wireless sensors. This advantage of the angular velocity-based AR model can potentially reduce the computation power and extend the lifetime of wireless sensor, which is usually powered by batteries. Many previous works have shown that the first three coefficients of the acceleration-based AR model are sensitive to the damage.[7,8,10,11] Hence, in following context, we choose the first coefficient of the angular velocity-based AR model ($\beta_1$) as the DSF.

The damage is declared by exploring the difference in means of DSFs before and after damage. Therefore, we can formulate the damage detection problem as a hypothesis test:

$$
\begin{aligned}
H_0 : \mu_{\text{DSF,undamaged}} &= \mu_{\text{DSF,test}} \\
H_1 : \mu_{\text{DSF,undamaged}} &\neq \mu_{\text{DSF,test}},
\end{aligned}
$$

where $\mu_{\text{DSF,undamaged}}$ is the mean of the DSFs extracted from the undamaged signal. This can be obtained either by simulation or by previous measurements. $\mu_{\text{DSF,test}}$ represents the mean of the DSFs from the test signal. Here, $H_0$ represents the undamaged status and $H_1$ represents the damaged status. We use $t$-test to justify the status.

## 3. EXPERIMENTAL VALIDATION

### 3.1 Description of Experiment

This experiment was designed and performed at National Center for Research on Earthquake Engineering (NCREE), Taiwan. Two identical three-story single bay steel frames were constructed. Both structures have an inter-story height of 1.1m. Floor dimension at every story is 1.1m × 1.5m. The columns have rectangular cross-sections with a dimension of 0.15m × 0.025m × 1.06m. Fig. 3 shows these two structures in the experiment facility. For Specimen 2, the Northwestern column (the red column in Fig. 4) is replaced with a weakened column, which has a thickness of 0.015m. Thus, Specimen 1 is a symmetric structure while Specimen 2 is non-symmetric.

These two structures were placed side by side on the same shake table. The record of the 1999 Chi-Chi earthquake Station TCU 071 was used as the base excitation of the experiment. The excitation was applied in

Figure 3. Photo of two structures (in green) on the shake table. The front structure is Specimen 1 and the back structure is Specimen 2.

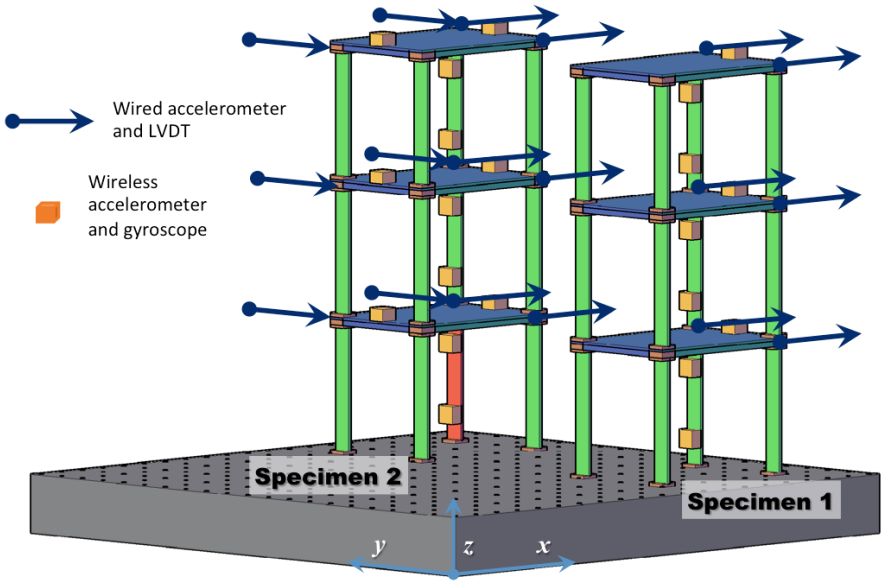


Figure 4. Two structures and sensor locations used at the NCREE experiment. The weakened column is in red.

the x-direction with amplitudes progressively increasing from 100 to 1450 gal. White noise excitations with 50 gal amplitude were applied between strong motion runs. Total 24 runs were conducted during the experiment. The details about each run are summarized in Table. 1. For the runs before Run WN11, a 500 kg mass block was placed on every story of both specimens. For the rest runs, an additional 500 kg mass block was added on the roof of each specimen.

Table 1. Summary of Runs. The attribute WN means the run is ambient vibration.

| Run number | Amplitude (gal) | Run number | Amplitude (gal) |
|---|---|---|---|
| WN1 | 50 | WN7 | 50 |
| 1 | 100 | 7 | 1000 |
| WN2 | 50 | WN8 | 50 |
| 2 | 250 | 8 | 1150 |
| WN3 | 50 | WN9 | 50 |
| 3 | 400 | 9 | 1300 |
| WN4 | 50 | WN10 | 50 |
| 4 | 550 | 10 | 1450 |
| WN5 | 50 | WN11 | 50 |
| 5 | 700 | 11 | 850 |
| WN6 | 50 | WN12 | 50 |
| 6 | 850 | 12 | 1000 |

### 3.2 Data Acquisition Systems

In this experiment, 21 wireless sensors were installed for data acquisition. Each wireless sensing device was assembled with a Telosb mote[12,13] and a 16-bit digital sensor, including a three-axis accelerometer and a three-axis gyroscope,[14] as shown in Fig. 5. These motes were operating within the SnowFort system, an open source wireless sensor system designed for infrastructure monitoring.[6,15] Motes and sensors were powered by two standard AA batteries. Both the accelerometer and gyroscope data were collected at 51.2Hz sampling frequency and filtered with a 20Hz anti-aliasing filter. The sampling frequency is fractional because the onboard microprocessor used 1024 ticks to represent one second and we set the mote to sample every 20 ticks. For the runs before Run WN10, the wireless accelerometers had a measurement range of $\pm$2g. The sensitivity was 16384 least significant bits (LSB) per g. The gyroscopes had a range of $\pm$250 degrees per second ($^\circ$/sec) with a sensitivity of 131 LSB per $^\circ$/sec. For the rest runs, the ranges of both accelerometer and gyroscope were increased. The range of accelerometer was increased to $\pm$8g with a sensitivity of 4096 LSB/g. The range of gyroscope was $\pm1000^\circ$/sec with a sensitivity of 32.8 LSB per $^\circ$/sec. According to Ref. 14, the accelerator has an average noise level of 1.265 mg, and the gyroscope has an average noise level of $0.016^\circ$/sec. The sampling of the accelerometer and gyroscope over all three axes is synchronized by sharing the same clock on the mote. Different motes are synchronized with a common base station.

The sensor installation locations are shown in Fig. 4. The wireless sensors were placed on the floors and the columns. The sensors on the columns were about 0.28m and 0.83m above each floor level to avoid hinged region. The wireless sensors, which were installed on the floors, were located at the midpoints of opposite edges of each floor. Since all wireless sensors were three-axis, the vibrations and rotations along all directions were collected.

### 3.3 Experimental Results

In this section, we will use the DSFs extracted from the measurements collected from the sensors on the columns. We want to investigate if a difference in mans can be identified for the pair of sensors at the exact same location of both specimens. As we have discussed above, Specimen 2 has a weaken column. Therefore, we can regard Specimen 1 as the undamaged structure and Specimen 2 as the damaged structure. If a difference in means is observed, we will declare the damage. Fig. 6 shows an example of the gyroscope measurements. We can see that the z-axis has the largest variation because the force is applied in the x-axis and the z-axis is perpendicular to the shake table.

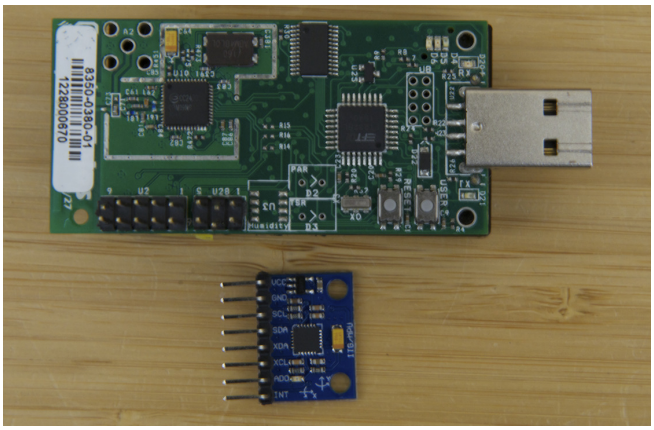

Figure 5. The green device (upper) is the Telosb mote with TI MSP430 microprocessor and CC2420 Zigbee transceiver. The blue device (lower) is the MPU 6050 digital sensor with one three-axis accelerometer and one three-axis gyroscope.

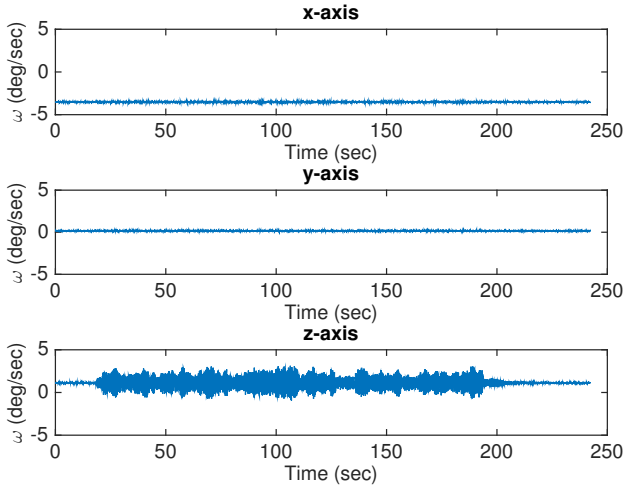


Figure 6. Gyroscope measurements of the sensor on the 1st floor column of Specimen 1 in Run WN1.

To extract the DSF from the gyroscope measurements, we divide the discrete time data into chunks with a chunk size of 200 samples. Each chunk is fitted with an AR model with an order of 5. As shown in Fig. 6, several samples at the beginning and the end of the recording were collected when the shake table was off. Therefore, we do not include these samples into the AR fitting process. In the following analysis, we use $\beta_1$ as the DSF. Fig. 7 shows the histogram of $\beta_1$, which approximates to a Gaussian distribution. This observation is consistent with our discussion in Section 2.

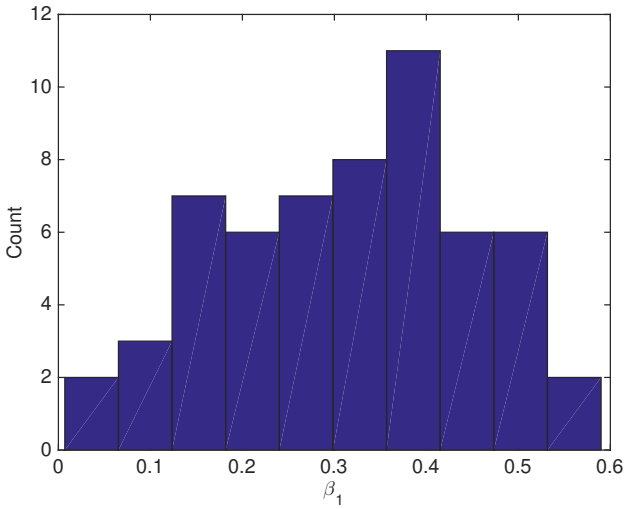


Figure 7. Histogram of $\beta_1$ collected from the sensor on the 1st floor column of Specimen 1 in Run WN1.

Fig. 8, 9, and 10 illustrate the box plots of the DSF $\beta_1$ collected at various locations of both Specimen 1 and Specimen 2. The box plot summarizes the median, 25% quantile, 75% quantile and other information. Since the DSF follows a Gaussian distribution, the median and mean are the same. For $t$-test, the significance level is set at 0.05. For the 1st floor columns, as shown in Fig. 8, the difference in means is statistically significant. For the 2nd floor columns, we have the consistent observation. For the 3rd floor columns, the $p$-value of one pair of sensors is larger than 0.5 and the difference in means is insignificant. The reason is that the sensor installation location is far away from the damage point. Therefore, the damage at the 1st floor has less effect on this pair of sensors.

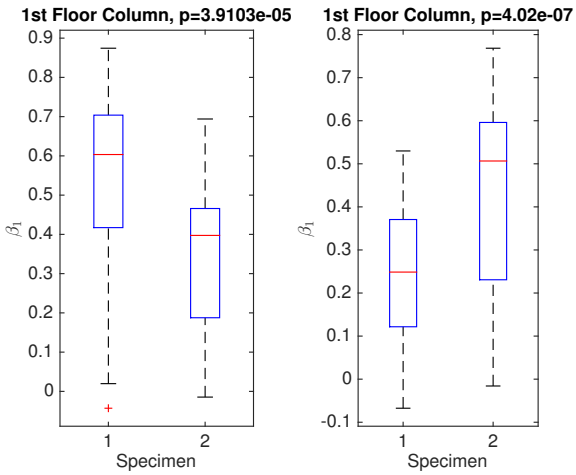


Figure 8. Box plot of $\beta_1$ of the sensor on the 1st floor columns of both specimens in Run WN1.

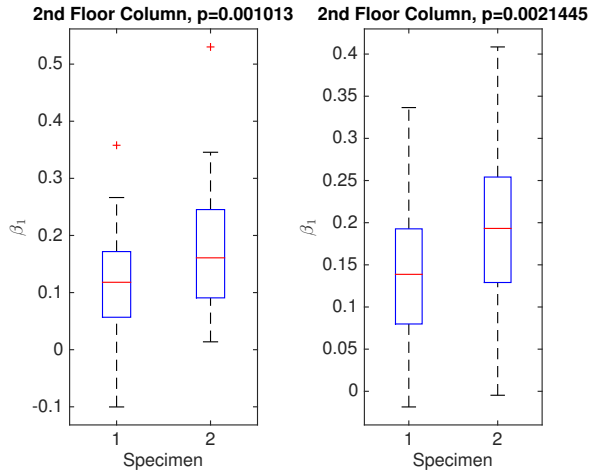


Figure 9. Box plot of $\beta_1$ of the sensor on the 2nd floor columns of both specimens in Run WN1.

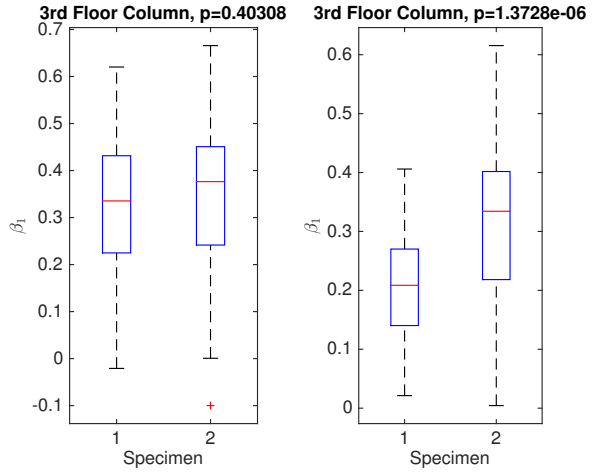


Figure 10. Box plot of $\beta_1$ of the sensor on the 3rd floor columns of both specimens in Run WN1.

## 4. CONCLUSION

In this paper, we present a damage detection algorithm based on the newly available angular velocity data. We firstly model the time-series angular velocity measurements as an AR model. Then we show that the angular velocity-based and acceleration-based AR models have a linear relationship and share many common properties. Therefore, as same as many vibration-based damage detection algorithms, we can use the difference in means of the DSFs to identify damage. At last, we use an experimental data set to validate that the angular velocity-based DSFs are sensitive to damage and the difference in means is statistically significant.

## ACKNOWLEDGMENTS

We would like to thank the researchers involved with the experiments, Dr. Chia-Ming Chang and Dr. Shu-Hsieng Chow from NCREE, and graduate students Shieh-Kung Huang, Wei-Ting Hsu, Chun-Kai Chan, Tzu-Yun Hung and Sheng-Fu Chen from National Taiwan University (NTU) for their overall help and collaboration. We also thank the personnel of the NCREE for their help and accommodation. The first author thanks Zhouyi Liao from Stanford University for helping perform the data cleansing. This research is partially supported by the NSF-NEESR Grant 1207911 and their support is gratefully acknowledged. The first author would like to thank the Charles H. Leavell Graduate Student Fellowship for the financial support.

## REFERENCES

[1] M. L. Fugate, H. Sohn, and C. R. Farrar, "Vibration-based damage detection using statistical process control," *Mechanical Systems and Signal Processing* **15**(4), pp. 707–721, 2001.

[2] W. Fan and P. Qiao, "Vibration-based damage identification methods: a review and comparative study," *Structural Health Monitoring* **10**(1), pp. 83–111, 2011.

[3] C. R. Farrar and K. Worden, *Structural health monitoring: a machine learning perspective*, John Wiley & Sons, 2012.

[4] S. Sung, J. Park, T. Nagayama, and H. Jung, "A multi-scale sensing and diagnosis system combining accelerometers and gyroscopes for bridge health monitoring," *Smart Materials and Structures* **23**(1), p. 015005, 2013.

[5] Z. Wu and S. Li, "Two-level damage detection strategy based on modal parameters from distributed dynamic macro-strain measurements," *Journal of Intelligent Material Systems and Structures* **18**(7), pp. 667–676, 2007.

[6] Y. Liao, M. Mollineaux, R. Hsu, R. Bartlett, A. Singla, A. Raja, R. Bajwa, and R. Rajagopal, "Snowfort: An open source wireless sensor network for data analytics in infrastructure and environmental monitoring," *Sensors Journal, IEEE* **14**, pp. 4253–4263, Dec 2014.

[7] K. K. Nair, A. S. Kiremidjian, and K. H. Law, "Time series-based damage detection and localization algorithm with application to the asce benchmark structure," *Journal of Sound and Vibration* **291**(1), pp. 349–368, 2006.

[8] Y. Liao and R. Rajagopal, "Message-passing sequential detection of multiple structural damages," in *12th International Conference on Applications of Statistics and Probability in Civil Engineering*, 2015.

[9] H. Sohn and C. R. Farrar, "Damage diagnosis using time series analysis of vibration signals," *Smart materials and structures* **10**(3), p. 446, 2001.

[10] H. Y. Noh, K. K. Nair, A. S. Kiremidjian, and C. Loh, "Application of time series based damage detection algorithms to the benchmark experiment at the national center for research on earthquake engineering (ncree) in taipei, taiwan," *Smart Structures and Systems* **5**(1), pp. 95–117, 2009.

[11] K. K. Nair and A. S. Kiremidjian, "Time series based structural damage detection algorithm using gaussian mixtures modeling," *Journal of Dynamic Systems, Measurement, and Control* **129**(3), pp. 285–293, 2007.

[12] J. Polastre, R. Szewczyk, and D. Culler, "Telos: enabling ultra-low power wireless research," in *Information Processing in Sensor Networks, 2005. IPSN 2005. Fourth International Symposium on*, pp. 364–369, IEEE, 2005.

[13] Moteiv, "Tmote sky datasheet." Data sheet, 2006.

[14] InvenSense, "Mpu-6000 and mpu-6050 product specification revision 3.4." Data sheet, 2013.

[15] SnowFort, "Snowfort website." Website, 2013. Accessed: 2015-10-29.